NREL
NATIONAL RENEWABLE ENERGY LABORATORY

Stability of CIGS Solar Cells and Component Materials Evaluated by a Step-Stress Accelerated Degradation Test Method

Preprint

F.J. Pern and R. Noufi

Presented at SPIE Optics + Photonics
San Diego, California
August 12–16, 2012

Conference Paper
NREL/CP-5200-54187
October 2012

Contract No. DE-AC36-08GO28308

NOTICE

Available electronically at http://www.osti.gov/bridge

Available for a processing fee to U.S. Department of Energy
and its contractors, in paper, from:

U.S. Department of Energy
Office of Scientific and Technical Information
P.O. Box 62
Oak Ridge, TN 37831-0062
phone: 865.576.8401
fax: 865.576.5728
email: mailto:reports@adonis.osti.gov

Available for sale to the public, in paper, from:

U.S. Department of Commerce
National Technical Information Service
5285 Port Royal Road
Springfield, VA 22161
phone: 800.553.6847
fax: 703.605.6900
email: orders@ntis.fedworld.gov
online ordering: http://www.ntis.gov/help/ordermethods.aspx

Cover Photos: (left to right) PIX 16416, PIX 17423, PIX 16560, PIX 17613, PIX 17436, PIX 17721

Printed on paper containing at least 50% wastepaper, including 10% post consumer waste.

STABILITY of CIGS solar cells and component materials evaluated by a step-stress accelerated degradation test method

F.J. Pern* and R. Noufi
National Center for Photovoltaics, National Renewable Energy Laboratory
1617 Cole Blvd., Golden, CO 80401, USA

ABSTRACT

A step-stress accelerated degradation testing (SSADT) method was employed for the first time to evaluate the stability of $CuInGaSe_2$ (CIGS) solar cells and device component materials in four Al-framed test structures encapsulated with an edge sealant and three kinds of backsheet or moisture barrier film for moisture ingress control. The SSADT exposure used a 15°C and then a 15% relative humidity (RH) increment step, beginning from 40°C/40%RH (T/RH = 40/40) to 85°C/70%RH (85/70) as of the moment. The voluminous data acquired and processed as of total DH = 3956 h with 85/70 = 704 h produced the following results. The best CIGS solar cells in sample Set-1 with a moisture-permeable TPT backsheet showed essentially identical I-V degradation trend regardless of the Al-doped ZnO (AZO) layer thickness ranging from standard 0.12 μm to 0.50 μm on the cells. No clear "stepwise" feature in the I-V parameter degradation curves corresponding to the SSADT T/RH/time profile was observed. Irregularity in I-V performance degradation pattern was observed with some cells showing early degradation at low T/RH < 55/55 and some showing large Voc, FF, and efficiency degradation due to increased series Rs (ohm-cm^2) at T/RH ≥ 70/70. Results of (electrochemical) impedance spectroscopy (ECIS) analysis indicate degradation of the CIGS solar cells corresponded to increased series resistance Rs (ohm) and degraded parallel (minority carrier diffusion/recombination) resistance Rp, capacitance C, overall time constant Rp*C, and "capacitor quality" factor (CPE-P), which were related to the cells' p-n junction properties. Heating at 85/70 appeared to benefit the CIGS solar cells as indicated by the largely recovered CPE-P factor. Device component materials, Mo on soda lime glass (Mo/SLG), bilayer ZnO (BZO), AlNi grid contact, and CdS/CIGS/Mo/SLG in test structures with TPT showed notable to significant degradation at T/RH ≥ 70/70. At T/RH = 85/70, substantial blistering of BZO layers on CIGS cell pieces was observed that was not seen on BZO/glass, and a CdS/CIGS sample displayed a small darkening and then flaking feature. Additionally, standard AlNi grid contact was less stable than thin Ni grid contact at T/RH ≥ 70/70. The edge sealant and moisture-blocking films were effective to block moisture ingress, as evidenced by the good stability of most CIGS solar cells and device components at T/RH = 85/70 for 704 h, and by preservation of the initial blue color on the RH indicator strips. The SSADT experiment is ongoing to be completed at T/RH = 85/85.

Key words: Step-stress accelerated degradation test (SSADT), encapsulated test structure, CIGS solar cell, Mo on SLG, Al-doped ZnO window layer, AlNi contact grid, damp heat stability, performance reliability

1. INTRODUCTION

Recent research advance has resulted in an efficiency improvement of $CuInGaSe_2$ (CIGS) thin-film solar cells from 20% to 20.3% [1-3]. Long-term performance reliability of thin-film PV modules, including CIGS, remains an important issue due to considerably high failure rate [4,5], particularly during the strenuous damp heat (DH) exposure test at 85°C and 85% RH for 1000 h according to the IEC 61646 qualification test requirement. CIGS solar cells and their device components, including Mo, ZnO, and AlNi contact grid, have been shown to be DH-sensitive or unstable [6-11]. DH-induced degradation of Al-doped ZnO (AZO) conductive window layer was reported to be performance-limiting factor for CIGSS mini-modules [12,13]. When tested in dry heat, e.g., 85°C and ~10% RH, CIGS solar cells showed good stability [14].

To screen or determine a material or device performance stability within a reasonable time frame, accelerated degradation or life test (ADT or ALT) is typically employed using constant or steady conditions; for example, DH exposure at 85°C and 85% RH has been commonly used in the IEC 61215 and IEC 61646 for PV modules. A constant ADT or ALT has the advantage of being simple and straight and is capable of screening or ranking test subjects in a

* john.pern@nrel.gov; phone 1 303 384-6615; fax 1 303 384-6490; www.nrel.gov/pv

fairly short period of time by using high stress conditions (e.g., temperature, RH, and pressure). However, the test may require either several test chambers or several runs and very long test time if working with one chamber to conduct under different conditions, especially with the objective to acquire activation energy for a given degradation mode. In comparison, a step-stress ADT or ALT (SSADT or SSALT)—the two are essentially the same in terms of reliability testing because both use the cumulative damage model—increases the stress condition(s) typically in a step-up manner during the course of test. This can offer the benefits of using a single test chamber to complete a test using multiple condition changes within a reasonable period of time. Suhir has discussed the various aspects of ALT, model equations, and application of ALT in microelectronic and photonic devices [15,16]. Khamis compared the use of constant and step-stress test for Weibull models [17], and Tseng and Wen reported their work using SSADT for highly reliable products [18]. Jones, Lee and coworkers promoted at NREL the applications of SSADT/SSALT to evaluate performance reliability of PV devices and modules [19,20] and presented recently their modeling and testing plan [21,22].

A SSADT method was employed in this work for the first time, in part based on discussion of a previous proposal [19], to evaluate the stability of CIGS solar cells and component materials in four encapsulated, edge-sealed test structures. While the four sides of the test structures were sealed with a desiccant-type edge sealant to block moisture, the test structures incorporated a piece of backsheet or moisture barrier film on the bottom side that allowed moisture ingress control with known water vapor transmission rate (WVTR) [23,24]. Three films were used: a moisture-permeable primed Tedlar/PET/Tedlar (TPT) backsheet, a Tedlar/Al foil/PET/EVA (TFPE) backsheet with an embedded moisture-blocking Al thin (0.7 mil) foil, and a transparent FG-200 moisture-barrier cover film. In addition to evaluating the usefulness of SSADT, the multiple purposes of this work and experiment design were to determine the threshold temperature (T) and RH that would induce significant material or cell degradation, the protection efficacy of moisture barrier film (TFPE and FG-200), the durability of the edge sealant, and, ultimately if successful, the T- and RH-dependent degradation activation energy. The latter would be applied to perform service life prediction based on the Peck equation, which in effect was an Eyring equation expanded and modified for modeling the time-to-failure in the T-RH bias conditions [15]. We reported previously the stability of CIGS solar cells, device components, and contact materials (Ag paste and solder alloy) exposed to constant DH at 85/85 either bare or in encapsulated test structure with TPT and FG-200 films [23,24]. At the moment of this writing, the SSADT experiment has progressed from 40^{o}C/40%RH (simply 40/40) to 85^{o}C/70%RH (85/70) with a total accumulated exposure time of 4204 h. The plan is to complete the test at 85^{o}C/85%RH (85/85).

2. EXPERIMENTAL

Sample preparation. Details of making the encapsulated Al-framed test structures and electrical contacts and connections were described previously [23,24]. In this work, a group of four sample sets was prepared (Set-1 to Set-4) and each set contained a set of CIGS solar cells or device components. Table 1 gives the details of the sample sets and component matrix. Basically, CIGS solar cells, Mo on soda lime glass substrate (Mo/SLG), AZO and bilayer ZnO (BZO) window films on glass substrates, and CdS/CIGS/Mo/SLG pieces were included. Except for the CdS/CIGS/Mo/SLG pieces, all the samples had thin Au wires soldered for electrical connections for current-voltage (I-V) and (electrochemical) impedance spectroscopy (ECIS) measurements. Three contact patterns were used: the "standard" trident grid on 0.42 cm^2 cells; a special interdigitated "bi-grid" on larger CIGS cells (1.8~2.2 cm^2/cell), AZO/glass, and BZO/glass samples (see images in Figs. 2 and 3 below); and a simple, two narrow strips of solder alloy applied on four component samples, as indicated in the three grid-related columns in Table 1. The bi-grid contact pattern was designed to allow I-V and ECIS measurements for the solar cells as well as resistance measurements by ECIS for the AZO, BZO and Mo on glass substrates. "Standard 3.05-μm" AlNi grid metal and thin (0.1~0.2-μm) Ni grid on BZO/glass and CIGS solar cells were compared. The CIGS solar cells fabricated with the bi-grid contacts were low efficiency, being used mainly for testing BZO DH stability, although I-V and ECIS were still measured. WVTR data of the TPT backsheet from Madico were 7.8 and 142.8 g/m^2-day measured at 39/100 and 83/100, respectively. WVTR for the TFPE backsheet, also from Madico, was < 0.05 g/m^2-day at 84.5/100, below the detection limit of the MOCON Permatran-W 3/33 system. WVTR for the 2-dyad (two repeated layers) moisture barrier film, FG-200, from Materion Large Area Coatings based on Vitex Barix technology was < 5x10^{-3} g/m^2-day [25]. An edge sealant tape, gray SET LP101, from TruSeal was used. A RH indicator strip from Süd-Chemie Performance Packaging was included in Set-2, 3, and 4 as an in-situ humidity level indicator.

DH exposure. The term damp heat "DH" is used in a loose manner here to indicate humidity level and temperature, rather than refer to the specific condition at 85/85. Prior to the DH exposures, the edges of the sample sets were covered with 1"-wide Kapton tapes to minimize DH-induced corrosion on the solder spots and tab ribbon pieces. The SSADT process began at 40/40 with an increment step of 15°C first and then 15% RH (i.e., 40/40, 55/40, 55/55, etc.) in an ESPEC environmental chamber [26]. Figure 1 illustrates the T-RH-time step profile along with a linear plot of time line for each T/RH segment.

Table 1. Sample Matrix of the Four Encapsulated Al-Framed Sets

Set ID	Samples in Set	Sample ID	AZO (µm)	Grid Type	Grid Metal	Metal (µm)	Back Sheet
Set-1	Std Mo/SLG	Mo-6-1B			(2 solder strips)		Madico
	Std BZO/7059	BZO4-32	0.12	N/A	(2 solder strips)		TPT
	CdS/CIGS/Mo/SLG	C2529-22 (piece)					
	CIGS Cells	C2528-23	0.12	Std	AlNi	3/0.05	
	CIGS Cells	C2529-21	0.24	Std	AlNi	3/0.05	
	CIGS Cells	C2529-11	0.5	Std	AlNi	3/0.05	
Set-2	BZO/1737	BZO15 AlNi-1	0.12	Bi-Grid	AlNi	3/0.05	Madico
	BZO/1737	BZO18 Ni-1	0.12	Bi-Grid	Ni	0.2	TPT
	BZO/1737	BZO24 Ni-1	0.5	Bi-Grid	Ni	0.2	
	CdS/CIGS/Mo/SLG	C2430 (piece)					
	CIGS Cell	C2510-12A	0.12	Bi-Grid	AlNi	3/0.05	
	CIGS Cell	C2510-22A	0.12	Bi-Grid	Ni	0.2	
	CIGS Cell	C2510-32A	0.12	Bi-Grid	Ni	0.2	
	RH Indicator Strip						
Set-3	BZO/1737	BZO15 AlNi-2	0.12	Bi-Grid	AlNi	3/0.05	Materion
	BZO/1737	BZO18 Ni-2	0.12	Bi-Grid	Ni	0.2	FG-200
	BZO/1737	BZO24 Ni-2	0.5	Bi-Grid	Ni	0.2	
	CdS/CIGS/Mo/SLG	C2430 (piece)					
	CIGS Cell	C2510-12B	0.12	Bi-Grid	AlNi	3/0.05	
	CIGS Cell	C2510-22B	0.12	Bi-Grid	Ni	0.2	
	CIGS Cell	C2510-32B	0.12	Bi-Grid	Ni	0.2	
	RH Indicator Strip						
Set-4	Std Mo/SLG	Mo-6-1C			(2 solder strips)		Madico
	AZO/7059	AZO11 AlNi-3	0.12	Bi-Grid	AlNi	3/0.05	TFPE
	BZO/1737	BZO15 AlNi-3	0.12	Bi-Grid	AlNi	3/0.05	
	AlNi Film/BZO	AlNi Film-1/BZO15			AlNi	3/0.05	
	CdS/CIGS/Mo/SLG	C2529-22 (piece)					
	CIGS Cell	C2528-13 (3 cells)	0.12	Bi-Grid	Ni	0.1	
	RH Indicator Strip						

Note 1: All CIGS solar cells and bilayer ZnO have a 0.1-µm i-ZnO layer

Characterization. The T-RH stability of the samples was monitored at least three times in each step segment. Photographs were taken each time the sample sets were removed from the ESPEC chamber and allowed to cool and "stabilize" (dry out) for at least two days. To ensure reliable ECIS and I-V measurements, the solder spots on the tab ribbon pieces were either cleaned with a blade or re-soldered, and the tab ribbon pieces were replaced with new ones and

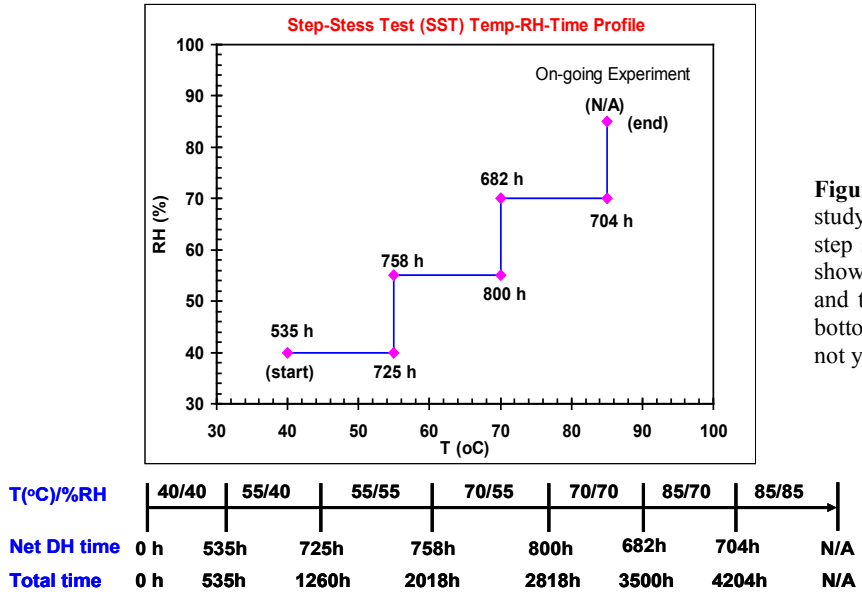

Figure 1. The T-RH step profile used in this study is shown in the top plot. Time for each step segment is indicated. The linear time line showing the T/RH, each step segment time, and the total accumulated time is given at the bottom. Time duration for 85/85 exposure is not yet available.

soldered when needed prior to ECIS measurements for both CIGS solar cells and component materials followed by I-V measurements for the solar cells [24]. Photoluminescence (PL) and electroluminescence (EL) imaging were also performed for CIGS solar cells and PL for CdS/CIGS/Mo/SLG pieces intermittently, due to limited availability of the systems as well as working personnel. The acquired images are still pending proper processing for normalization of the image light intensity and are therefore unavailable for discussion at the moment.

3. RESULTS AND DISCUSSION

Because the samples at DH = 4204 h have not been completed with all the measurements (except for the images photographed at DH 4204 h shown in Fig. 3 below) at the time of this writing, this paper will present only some of the main results from the large quantity of data that have been processed up to a total DH exposure time of 3956 h at 85/70 RH for 456 h. To simplify the expression, the exposure conditions, T, %RH and time, will be indicated as, for example, "a total DH = 3956 h (85/70 DH = 456 h)" in the following discussions. A more comprehensive report is expected after the experiment is completed with exposure at DH 85/85 in the near future. On the exposure T/RH condition, the SSADT experiment began at a low 40/40 to examine if CIGS cell and device components would show any notable sign of degradation. The exposure time for each step segment was somehow irregular. A relatively short period of 535 h at 40/40 was used because degradation at this condition, if any, was not expected to be substantial. Longer exposure time was given in 55/55 to 70/55 segments in hope to "catch" the significant degrading points. At higher T/RH, 70/70 and 85/70, a shorter time (~700 h) was used because degradation rate was expected to be greater. Although not yet conducted, final exposure at 85/85 is planned to complete in a similar period of ~700 h. The following discussions group the results into three main parts: Moisture ingress control, CIGS solar cells characterized by I-V and ECIS, and device components (Mo, ZnO, and AlNi contact) by ECIS. Effects of moisture ingress (i.e., via TPT) versus moisture blocking (FG-200 and TFPE) on the DH stability of test subjects will be compared in the discussion of each subject.

3.1 Moisture Ingress Control

Two materials were used on the four encapsulated Al-framed test structures to control the moisture ingress: an edge sealant (TruSeal LP101) around the perimeters between the glass cover plate and the Al frame, and a back sheet at the Al frame's bottom side being secured also by the edge sealant with a piece of 1/16" Al plate. Both the Al frame and the 1/16" Al plate had a 1.25-cm x 1.25-cm opening in the center. A RH indicator strip was included in Set-2, 3, and 4, but not in Set-1 because of space limitation. Although the RH indicator strip could not offer a precise reading of humidity level inside the encapsulated test structures, it did provide a qualitative indication. As illustrated in Fig. 2 for Set-2 with a TPT backsheet, the initial blue color on the RH indicator strip progressively changed its color to pink-brown as the T/RH increased from 40/40 to 85/70 over a total DH = 3956 h. The pink-blue color change was based on Co(II) hydration-dehydration and scaled from 10% to 100% humidity level. However, the strip changed to brownish after prolonged heating at 70°~85°C at 70%RH, likely affected by the strip paper, suggesting the shortcoming of using the RH strips in this kind of prolonged testing.

Figure 2. Photographs showing color changes on the RH indicated strip inside Set-2 with a TPT backsheet. The T/RH conditions, along with the total and segmental exposure times, are indicated at the bottom of each image, increasing stepwise from 40/40 to 85/70. Bi-grid contacts were used on the C2510 solar cells and BZO/glass samples.

Figure 3 shows photographs of the four sets with sample layouts and compares the color on the RH indicator strips. As seen, the blue color on the RH strips in Set-3 with a FG-200 and in Set-4 with a TFPE moisture barrier film remained unchanged even at a total DH = 4204 h and 85/70 DH = 704 h. This observation indicates that the FG-200 and TFPE films were able to block the moisture effectively up to 70% RH at 85°C. The results also indicate the sealing soundness and durability of the edge sealant, TruSeal LP101, which was able to withstand all the exposures as well as the handling over the course of 4204 h. The RH strip's blue color would have changed readily if there were any sealing leak around the perimeters on either set. Therefore, the samples inside Set-3 and Set-4 could be considered as having been exposed to dry heat. In a previous study, the blue color of the RH indicator strip in a "Dummy-2" set with FG-200 remained essentially unchanged after exposing at a constant 85/85 DH for > 1000 h, but changed to pink-brown quickly within ~250 h in a "Dummy-1" set with TPT [24]. It should be noted that the edge sealant, being a desiccant-type material, would absorb some moisture to certain level, therefore impeding the moisture saturation time inside the encapsulated structure. However, no quantitative evaluation was available or made for this hindrance.

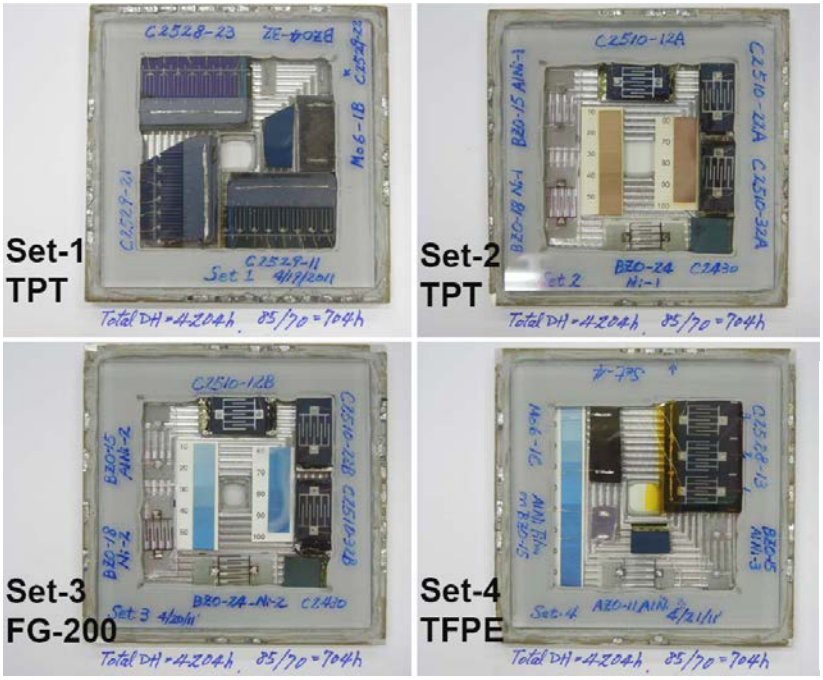

Figure 3. Photographs showing the four sets after a total DH = 4204 h and 85/70 DH = 704 h. The photographs also show the layout of different samples in each set as marked by handwriting. The films used for moisture ingress control are also indicated at the lower left corners: Set-1 and Set 2: TPT; Set-3: FG-200; Set-4: TFPE.

3.2 Stability of CIGS Solar Cells in SSADT

The SSADT stability of the CIGS solar cells in Set-1 is the primary focus of this part. As pointed out in the Experimental section, the CIGS cells with bi-grid contacts in Set-2, 3, and 4 were typically low efficiency and were used primarily for monitoring BZO degradation; although they were still I-V measured at each segment step, their results are not emphasized here. Figure 4 shows the Voc, Jsc, fill factor (FF), efficiency, and series Rs plots grouped for the five cells on C2528-23 coupon with 0.12 μm AZO as a function of total DH exposure time. (Cells with initially poor efficiency were not included.) Apart from cells # 1 and #5, the other three cells on C2528-23 displayed gradual decrease in Voc and stable Jsc until DH > 2818 h (70/55 DH = 800 h). Cell #4 was most stable, showing a small decrease until DH ≥ 3500 h (70/70 DH = 682 h) when series Rs started to increase. In comparison, cell #6 was less stable, showing an increase of Rs in early stage at DH =1494 h (55/55 DH = 234 h), resulting in corresponding drops in FF and efficiency. As seen in Fig. 4b, when compared to the initial Jsc ~28 mA/cm^2 at DH =0 h, cells #1 and #5 exhibited abnormal high Jsc (> 50 mA/cm^2) after being exposed to 40/40 for just 319 h, likely caused by "cross-talk" with neighboring regions or cells, either by incomplete device isolation during photolithographic processing and/or by certain "conductive link" induced by the moisture. Similar cross-talk contributing to unusual high Jsc was also observed in another study as reported [27]. The cross-talk consequentially affected other I-V parameters, more notably FF and efficiency, as seen in Fig. 4 (c and d). However the highly fluctuating curves in Rs plots for the two cells in Fig. 4e suggest the "conductive link" was unsteady.

The two cells also degraded faster up to DH = 2818 h (70/55 DH = 800 h) and then failed in the next exposure at 70/70 when total DH = 3028 h (Fig. 4d).

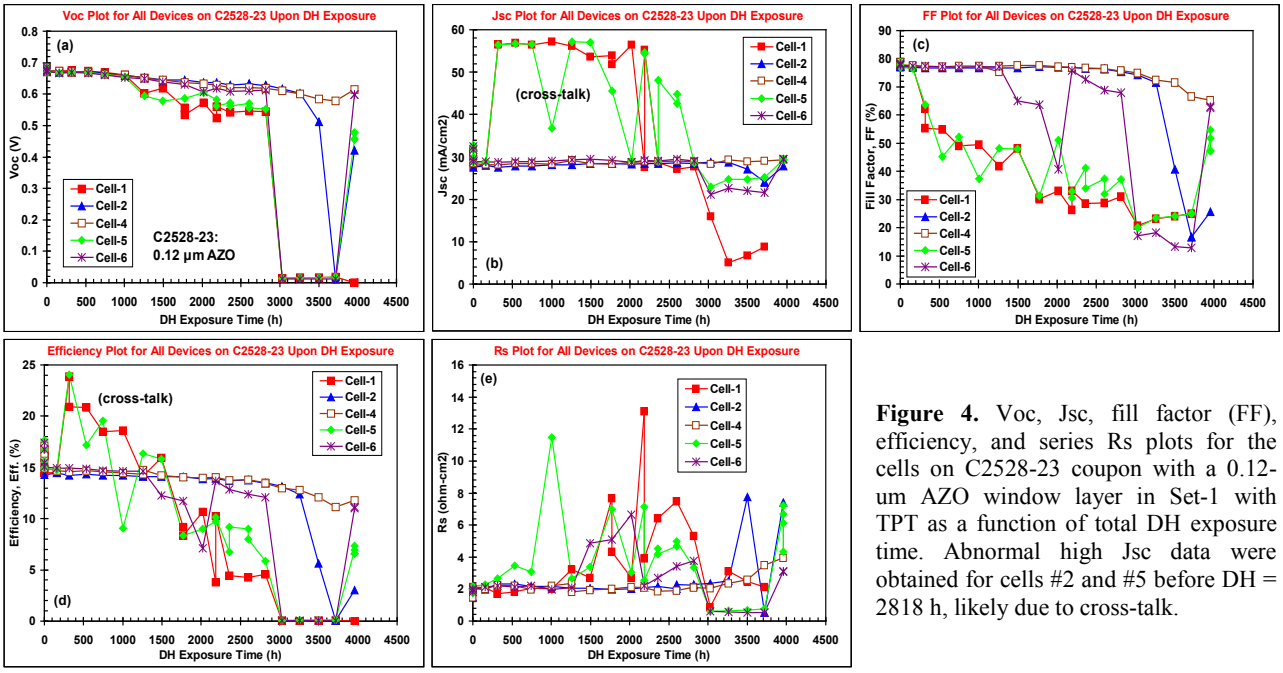

Figure 4. Voc, Jsc, fill factor (FF), efficiency, and series Rs plots for the cells on C2528-23 coupon with a 0.12-um AZO window layer in Set-1 with TPT as a function of total DH exposure time. Abnormal high Jsc data were obtained for cells #2 and #5 before DH = 2818 h, likely due to cross-talk.

Figure 5 shows the similar plots grouped for four cells on C2529-11 coupon with 0.50 µm AZO. While cell #6 was most stable with little change in Voc, Jsc, FF, and efficiency until DH ≥ 3500 h (70/70 DH = 682 h) when series Rs started to rise (Fig. 5e); cell #2 behaved similarly but started to show notable degradation in FF and efficiency at DH ≥ 2602 h (70/55 DH = 584 h) with a corresponding Rs increase. Compared to other three cells, cell #4 showed a lower FF and efficiency due to higher initial Rs, probably caused by soldering, but it was fairly stable until DH > 2602 h. Cell #7 was troubled with an early Rs increase (Fig. 5e) that decreased its FF and efficiency accordingly (Fig. 5c and 5d), but its Jsc

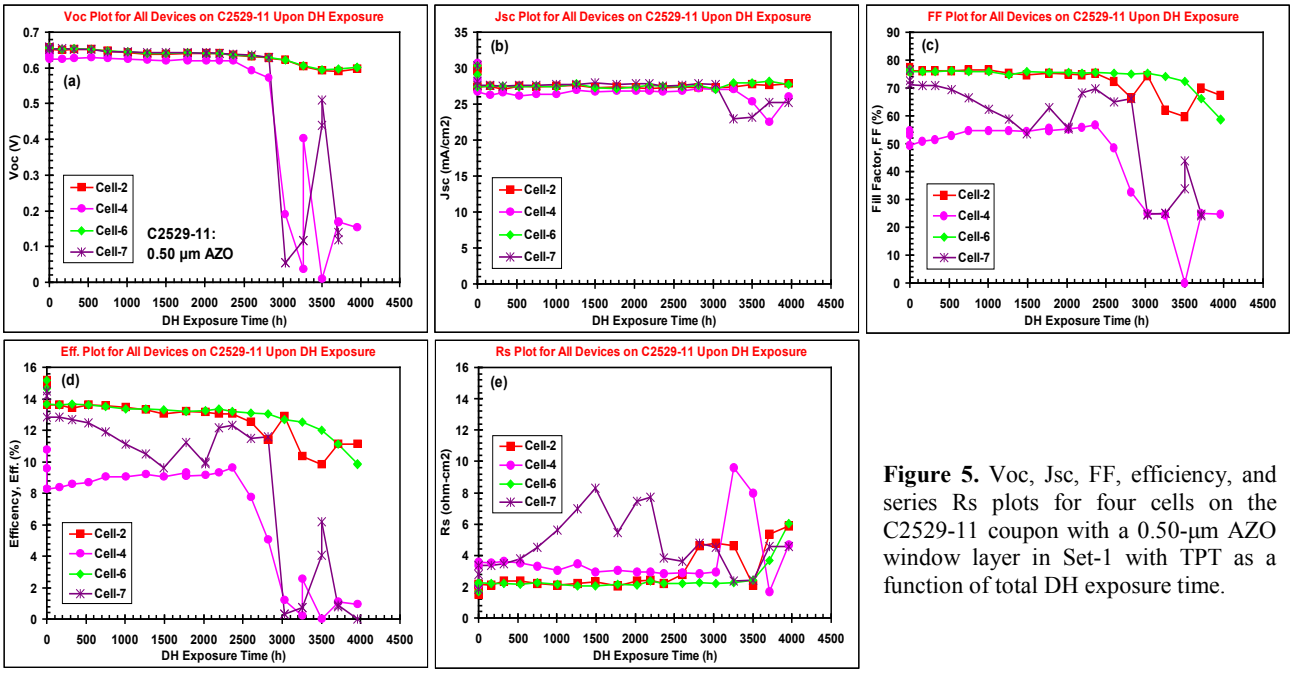

Figure 5. Voc, Jsc, FF, efficiency, and series Rs plots for four cells on the C2529-11 coupon with a 0.50-µm AZO window layer in Set-1 with TPT as a function of total DH exposure time.

changed little even at DH = 3956 h while Voc, FF, and efficiency precipitated largely at DH = 3028 h (70/70 DH = 210 h) but recovered briefly at 3500 h. The cell's electrical Rs was lowered at higher T/RH condition, suggesting the cell's large degradation at DH ≥ 3000h was not due to Rs but something else. The brief recovery at DH = 3500 h (70/70 DH = 682 h) could be a result of heating effect; more on this possibility will be discussed below.

Only three of the five cells on C2529-21 with 0.24 μm AZO were useful after cell #1 was damaged by soldering, which recovered gradually by ~50% in efficiency at DH = 2189 h (70/55 DH = 171 h) (not shown), and cell #2 was accidentally "electrocuted" by a high bias spike in EL measurement at DH = 319 h. Among the three useful cells, I-V data of cell #4 fluctuated irregularly, perhaps a result of Rs fluctuation (not shown). The best two cells, #3 and #5, are plotted along with the best cells from C2528-23 and C2529-11, as illustrated in Fig. 6. More notable degradation was seen on C2529-11 cell #2 and C2529-21 cell #5 at DH ≥ 2818 h (70/55 DH = 800 h, Fig. 6e) due to increased Rs, which affected FF and efficiency (Fig. 6c and 6d). The results in Fig. 6 also indicate that DH stability for the best cells in the current SSADT study was nearly identical, independent of AZO thickness. Similar results — no AZO thickness effect on DH stability of CIGS solar cells — were also observed in another study [27]. Furthermore, with Jsc curves staying essentially flat, the Voc, FF, and efficiency curves at DH < 3000 h (70/70 DH = 210 h) in Fig. 6 gradually declined and did not show clear degrading steps as one would expect SSADT or SSALT to generate; only at higher T/RH at DH > ~3000 h were more obvious degradation curves obtained. This observation raises an issue on what T/RH/time conditions should be chosen in a SSADT or SSALT experiment to produce the desired (or expected) stepwise degradation features for modeling analysis.

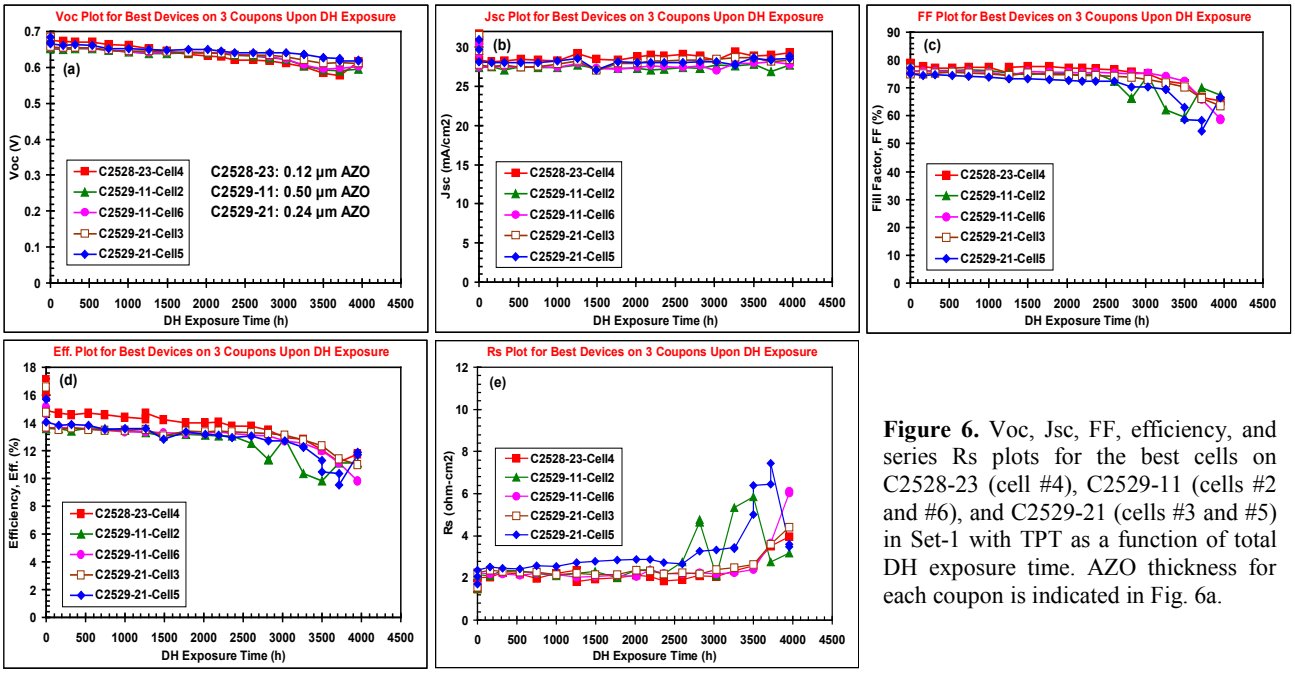

Figure 6. Voc, Jsc, FF, efficiency, and series Rs plots for the best cells on C2528-23 (cell #4), C2529-11 (cells #2 and #6), and C2529-21 (cells #3 and #5) in Set-1 with TPT as a function of total DH exposure time. AZO thickness for each coupon is indicated in Fig. 6a.

An interesting observation in a couple cases is that a CIGS solar cell, e.g., cell #1 on C2529-11 with 0.50 μm AZO and an initially poor efficiency, would gradually increase its Voc, Jsc, and efficiency significantly upon the lengthy DH exposure, while the Rs increase did not further reduce the initially low FF (figures not shown). The cause of this improvement is not clear, but probably due to heating effect on the cell. Additionally, apart from the "best cells" results shown in Fig. 6, some cells on the three coupons with different AZO thickness exhibited a significant degree of irregularity in degradation trend (rate and pattern) — some are shown in Figs. 4 and 5 above and some are not shown with initially moderate efficiency that degraded in a similar random manner. This observation indicates the presence of a relatively high degree of variation in cell stability during the course of SSADT, which is essentially the same as that was observed in another study under constant ADT at DH 85/85 [27], presenting again the challenge of conducting such reliability studies.

3.3 ECIS Analysis

All the CIGS solar cells and device components with external electrical contacts via the Au wires soldered on tab ribbon pieces on the four sample sets were also characterized with ECIS to derive the resistance and capacitance values. ECIS was employed in previous studies that produced useful information on cell characteristics and DH stability [23,24]. The basic principle, data acquisition and curve fit analysis were described in [24]. Essentially, the measured ECIS data files are curve fitted by a simple built-in "Randles cell" equivalent circuit (Rs–C//Rp) to obtain the series resistance Rs (ohm), parallel resistance Rp (ohm), and capacitance C or CPE-T (farad, F), where CPE is the constant phase element. The "overall" time constant is then calculated by the product of Rp*C (second, s), which is essentially equaled to the value calculated from $1/2\pi f$ using the frequency, f, at the top of the semicircle in Z" – Z' complex plot and corresponds (or is related) to the (effective) minority carrier lifetime according to Bisquert and coworkers [28-30]. However, "chemical capacitance," C_{μ}, being separated from the "double layer capacitance," C_{dl}, beyond certain forward bias, should be used to more reliably derive the minority carrier lifetime [28]. Because the capacitance C (or CPE-T) derived from curve fitting of the Z"-Z' semicircles in this work is an "overall" magnitude, without trying to separate the recombination and diffusion terms (i.e., C_{μ} and C_{dl}), therefore the Rp*C will be referred to simply as the overall time constant (or "lifetime") here, similar to that used previously [24]. Furthermore, in curve-fitting the R-C circuit, a "capacitor quality" parameter, CPE-P, can be obtained: CPE-P = 1.0 for an ideal capacitor, < 1.0 for a "depressed" capacitor, and 0.0 for a resistor. More details on ECIS analysis and its applications for different types of solar cells including CIGS, as well as explanations of CPE are available in the literature [28-35].

Figure 7 illustrates the ECIS parameter plots for three best cells on the three CIGS cell coupons in Set-1 obtained at 0.25-V bias as a function of total DH exposure time; their I-V parameter plots vs. DH time are given in Fig. 6 above. In Fig. 7(a, c, and e), the three cells' series resistance, Rs (derived from curve fitting), was very close to the measured impedance Z' at 1M (10^6) Hz, while the parallel Rp was essentially superimposed with Z' at 1 Hz, which would be the sum of Rs and Rp. (Typically Rs << Rp on a solar cell.) All Rs (and Z' at 1M Hz) showed a gradual increase over the

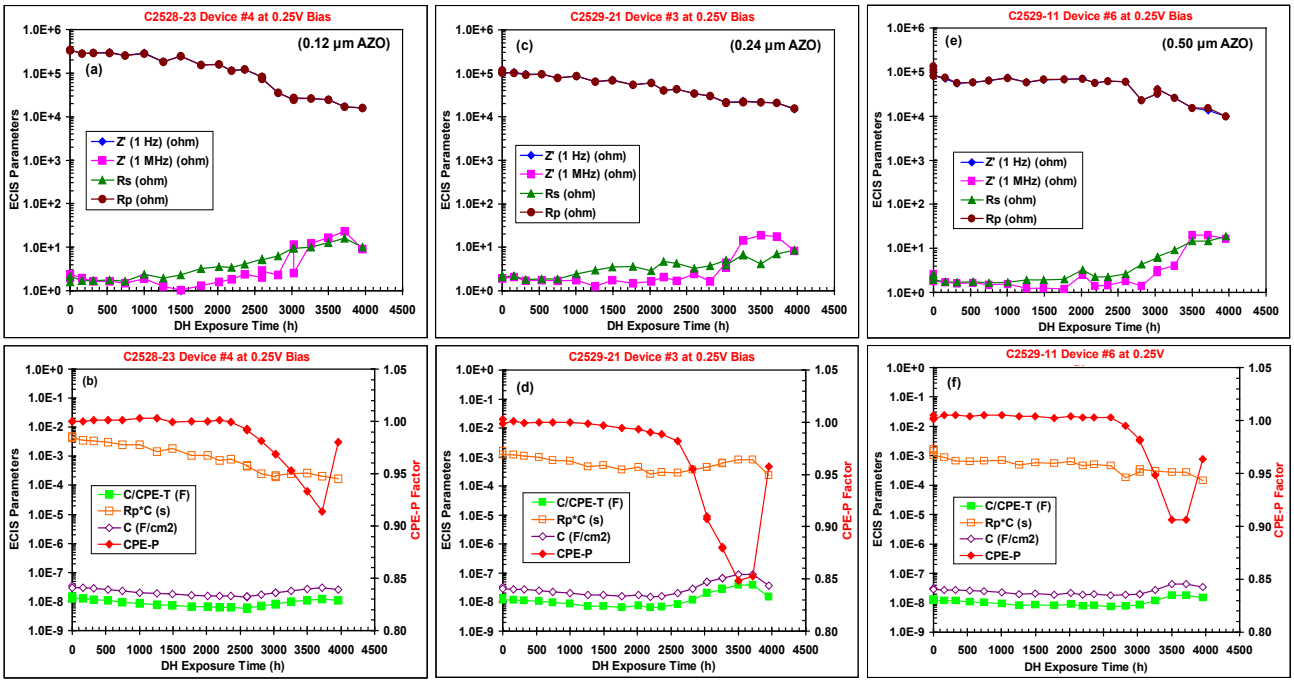

Figure 7. ECIS parameter plots as a function of total DH exposure time for three best cells, cell #4 on C2528-23 with 0.12 µm AZO, cell #3 on C2529-21 with 0.24 µm AZO, and cell #6 on C2529-11 with 0.50 µm AZO. (a, c, d) impedance and resistance plots in *semi-log* scale: Z' at 1M Hz = series resistance, Rs (ohm), and Z' at 1 Hz = Rs + Rp, parallel resistance. Z' (1 Hz) curves are not readily seen because they are overlapped with the Rp curves. (b, d, f) Plots of capacitance, C and CPE-T and time constant (lifetime), Rp*C, in *semi-log* scale (left Y axis), and plots of "capacitor quality" factor, CPE-P, in *linear* scale (right Y axis). Z' data were actually measured; Rs, Rp, C, and CPE-P were derived from curve-fit of the ECIS data files using a simple Rs–Rp//C equivalent circuit; and Rp*C data were calculated. The three cells' I-V parameter plots are shown in Fig. 6.

course of DH exposure, similar to the trends of series Rs (ohm-cm^2) from light I-V measurements as seen in Fig. 6e. Meanwhile, a gradual decrease was seen on the parallel Rp, an indicator of "diffusion and recombination resistance" of minority carriers at the p-n junction of a solar cell (represented as an Rs–C//Rp equivalent circuit) [28-30]. The effective lifetime Rp*C declined correspondingly, while the capacitance C or CPE-T (in F or F/cm^2 if divided by the cell area 0.42 cm^2) showed a slow decline to DH ~ 2500 h (Fig. 7b and 7d) or ~ 3000 h (Fig. 7f) before showing a gain then a drop again in later stage. In the meantime, the CPE-P factors remained steady (Fig. 7b, 7f) or exhibited a small decline (Fig. 7d) up to DH ~ 2600 h (70/55 DH = 584 h) for all three best cells, followed by a rapid drop between DH = 2600 h and 3500 h (70/70 DH = 682 h) before recovering significantly afterwards (85/70 DH = 456 h).

These results indicate that the I-V performance of the three best cells were degraded by an increase in series resistance and a decrease in Rp, C (and Rp*C), and CPE-P due to degraded and possibly "depressed" p-n junction and depletion width when exposing to DH. The degradation rate was fairly small or slow when T/RH < 70/55 (DH < 2600 h), but was much faster when T/RH = 70/70. The three cells' capacitor quality was largely recovered after the cells were exposed to 85^{o}C (DH > 3500 h), as indicated by improved CPE-P and C, suggesting the beneficial effect of heating to the solar cells as also mentioned above. However, the gains in CPE-P and C were offset negatively by the continuously increasing Rs and decreasing Rp at 70%–85% RH, and could not result in a recovery in cell efficiency.

3.4 Stability of Device Components in SSADT

The SSADT DH stability of CIGS device components, namely Mo/SLG, Al-doped ZnO (AZO), bilayer ZnO (BZO), AlNi grid contact, and CdS/CIGS/Mo/SLG pieces, was also evaluated in encapsulated test structures seen in Fig. 3.

3.4.1 Mo on SLG (Mo/SLG)

The stability of bare Mo/SLG in damp heat (85/85) was investigated previously [6]. Substantial flaking (as seen in SEM), corrosion, and color change on Mo were typically observed along with becoming highly resistive after 100~200 h at 85/85 DH exposure. Dry heat (85/~10) normally did not cause notable degradation on Mo. The Z' resistance (impedance) results for Mo/SLG in Set-1 (TPT) and in Set-4 (TFPE) are compared in Fig. 8. To measure the resistance across the 0.7-µm thick Mo film, two narrow solder strips separated by ~18 mm were applied with Au wires attached. As seen in Fig. 8a, the Mo/SLG in Set-1 (TPT) showed fairly stable resistance up to DH = 3716 h (85/70 DH = 216 h), but became highly resistive (not measurable) beyond that point. In the meantime, the color changed to darkening brown with small white dots starting to appear on the surface after DH > 3500 h, as illustrated by the photograph insert in Fig. 8a for the sample at DH = 3956 h (85/70 DH = 456 h). Similar white dots were also observed in a previous sample, "Dummy-1" (TPT), which was exposed to constant 85/85 DH = 1015 h [24]. The DH-induced corrosion and resistance increase was not observed for the Mo/SLG sample in Set-4 (TFPE), however. The difference clearly demonstrates that the TFPE film was effective to prevent the DH-sensitive Mo from being corroded up to 85/70 DH = 704 h. Whether TFPE is effective to block moisture at 85/85 remains to be verified when the experiment is completed later.

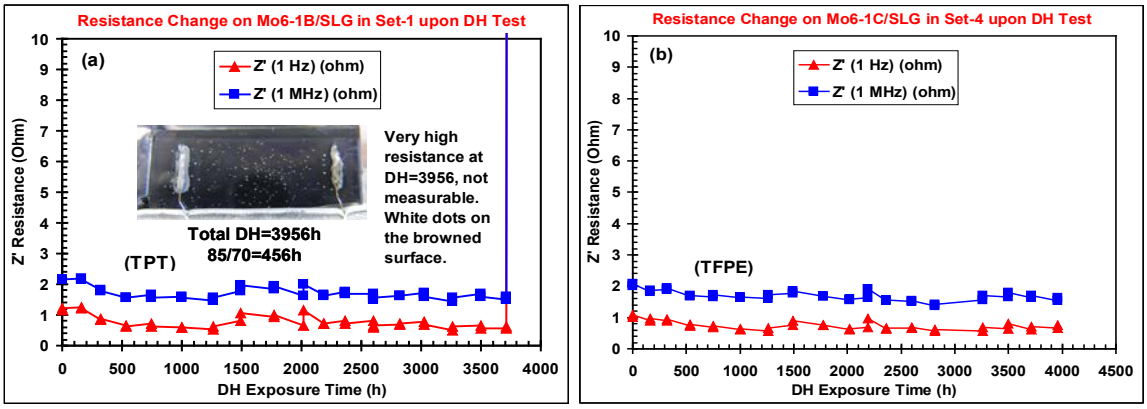

Figure 8. Z' resistance plots for Mo/SLG sample in (a) Set-1 with a TPT backsheet and (b) Set-4 with a TFPE backsheet. Z' data at 1 Hz and 1 Mz were shown, where a small difference is present due to intrinsic capacitance on the contacts. The photograph insert in (a) shows the two solder strips/Au wire contacts and the small white dots on Mo surface at total DH = 3956 h (85/70 DH = 456 h).

3.4.2 BZO/AlNi and BZO/Ni on cells and glass substrates

The bilayer ZnO (BZO) was tested either as stand alone on glass substrates or on CIGS solar cells. A special "bi-grid" contact pattern was used on most of the BZO and CIGS cell pieces (Fig. 3) that allowed independent I-V and ECIS measurements. Electrical contact on one sample, BZO4-32/glass, used two solder strips, same as that on Mo/SLG, which would produce a resistance much higher than that with a bi-grid. To compare with the standard AlNi contact material, thin (0.1~0.2 μm) Ni on BZO/glass or BZO/CIGS solar cells was also investigated.

Figure 9 compares the Z' resistance results for five BZO/glass in three sample sets: BZO4-32 with solder strip contacts in Set-1 (TPT), a pair of BZO-15 with standard 3.05-μm AlNi contact bi-grid and BZO-24 with 0.2 μm Ni in both Set-2 (TPT) and Set-3 (FG-200), respectively (see Fig. 3 images with each sample ID marked). The results show that BZO-4 in Set-1 (TPT) with solder strip contacts started to increase its resistance gradually at DH > 1000 h (55/40) and showed a large jump after DH > 3500 h (70/70 DH = 682 h) from ~100 ohms to ~145 ohms at DH = 3956 h (Fig. 9a). In comparison, BZO-15 in Set-2 (TPT) with standard AlNi grid contact showed an unsteady but increasing resistance after DH > 2818 h (70/55), Fig. 9b, but BZO-24 with thin Ni grid was fairly stable in Set-2 (TPT), despite some data scattering, Fig. 9c. The differences among the three BZO/glass samples indicate that the BZO resistance change was not clearly detected with the bi-grid contact likely due to small separation between the gridlines (1 mm, as compared with the 18-mm distance of the solder strips) and that the AlNi grid contact with BZO-15 also started to degrade unsteadily at DH = 3028 h (70/70 DH = 210 h) and more obviously at DH = 3716 h (85/70 DH = 216 h). We previously reported a very large resistance increase on bare (unencapsulated) BZO/glass samples with standard AlNi bi-grid exposed to constant 85/85 DH = 100 h and nearly linear resistance increase with respect to time on a BZO/glass sample in a similarly encapsulated Dummy-1 (TPT) also exposed to constant 85/85 DH > 1200 h [24]. Corrosion of AlNi grid on the bare BZO/glass samples was observed but not on thin Ni grid [24]. In Set-3 with moisture barrier film FG-200, BZO-15 (AlNi) and BZO-24 (Ni) samples remained essentially unchanged as seen in Fig. 9(d and e) at DH = 3956 h (85/70 DH = 456 h). Similar stability was observed for AZO/glass and BZO/glass samples in a Dummy-2 (FG-200) exposed to constant 85/85 DH > 1200 h [24].

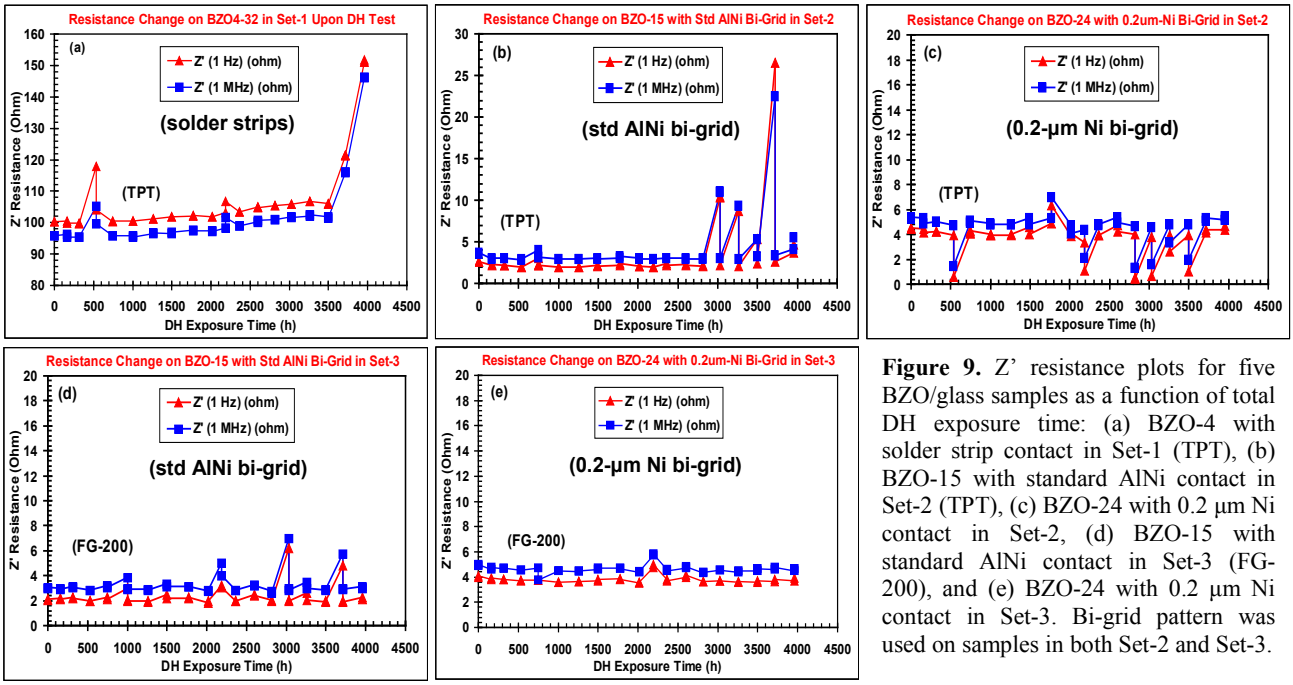

Figure 9. Z' resistance plots for five BZO/glass samples as a function of total DH exposure time: (a) BZO-4 with solder strip contact in Set-1 (TPT), (b) BZO-15 with standard AlNi contact in Set-2 (TPT), (c) BZO-24 with 0.2 μm Ni contact in Set-2, (d) BZO-15 with standard AlNi contact in Set-3 (FG-200), and (e) BZO-24 with 0.2 μm Ni contact in Set-3. Bi-grid pattern was used on samples in both Set-2 and Set-3.

The SSADT DH stability of BZO window layer on CIGS solar cells was also monitored in-situ by ECIS measurements along with the typical I-V measurements for the solar cells. The ECIS measurements were conducted through the bi-grid contacts, which also offered the flexibility to measure I-V via either one of the two contacts. Similar to the BZO/glass samples above, standard 3.05-µm AlNi contact and 0.1-µm Ni contact in the bi-grid pattern were used on some CIGS solar cells that were encapsulated in Set-2, 3, and 4 (Fig. 3). Figure 10(a and b) show the I-V parameter plots for the cells of C2510-12A in Set-2 (TPT) and C2510-12B in Set-3 (FG-200), and Fig. 10(c and d) show the Z' resistance plots for the BZO layers on the two cells as a function of total DH exposure time. On C2510-12A in Set-2 (TPT), obvious fluctuation and degradation in I-V parameters were noted (Fig. 10a), and the Z' resistance for the BZO measured via the AlNi bi-grid contacts displayed a small and gradual increase before DH ~ 3500 h but a quick rise afterward (Fig. 10c), similar to that seen in Fig. 9a. The FG-200 moisture barrier film on Set-3 provided good protection of C2510-12B cell and the BZO and AlNi grid on it — most of the I-V parameters and Z' resistance remained stable as of DH = 3956 h as seen in Fig. 10(b and d), except for Voc that showed a little decrease. By comparing Fig. 10c with Fig. 9b, the difference in Z' resistance changes in current SSADT exposure indicates that BZO sputtered on glass was relatively more DH-stable than BZO on CIGS solar cells, which was in good accord with the previous results, attributing to higher crystallinity on the former [23,27]. Furthermore, the BZO layers on C2510 cell pieces in Set-2 (TPT) showed darkening from one side (closer to the center opening with TPT) at early DH < 1772 h (55/55 DH = 512 h) that progressed further onto more cell areas as T/RH/time increased, and finally showed a large number of small "blistering" (i.e., an early sign of flaking) on C2510-12A and 22A pieces at DH = 4204 h (85/70 DH =704 h). In contrast, C2510 cell pieces in Set-3 (FG-200) did not show similar changes on the BZO layers.

The BZO on C2528-13 with 0.1-µm Ni bi-grid contacts in Set-4 (TFPE) exhibited a notable decrease in Z' resistance on cell #1 after DH > 1000 h (55/40) and stabilized at DH > 1772 h (55/55 DH = 512 h), Fig. 10e; the change was quite small on cell #3, Fig. 10f. It is not clear what caused the Z' resistance to decrease, but the result seems to suggest that the BZO/Ni grid contact was improved by dry-heating so the overall resistance was decreased. Additionally, a thicker (0.2 µm) Ni grid contact appeared to offer a lower resistance (~4 vs. 12 ohm) and better DH stability as well, when Fig. 10(e and f) were compared with Fig. 9(c and e). Also in Set-4 (TFPE), Z' resistance measured for 0.12-µm AZO-11/glass via the 3.05-µm AlNi bi-grid contacts displayed a notable early decrease before DH = 1000 h followed by small fluctuations after DH > 1000 h, while BZO-15/glass was relatively stable until DH > 3000 h, when a moderate fluctuation was seen

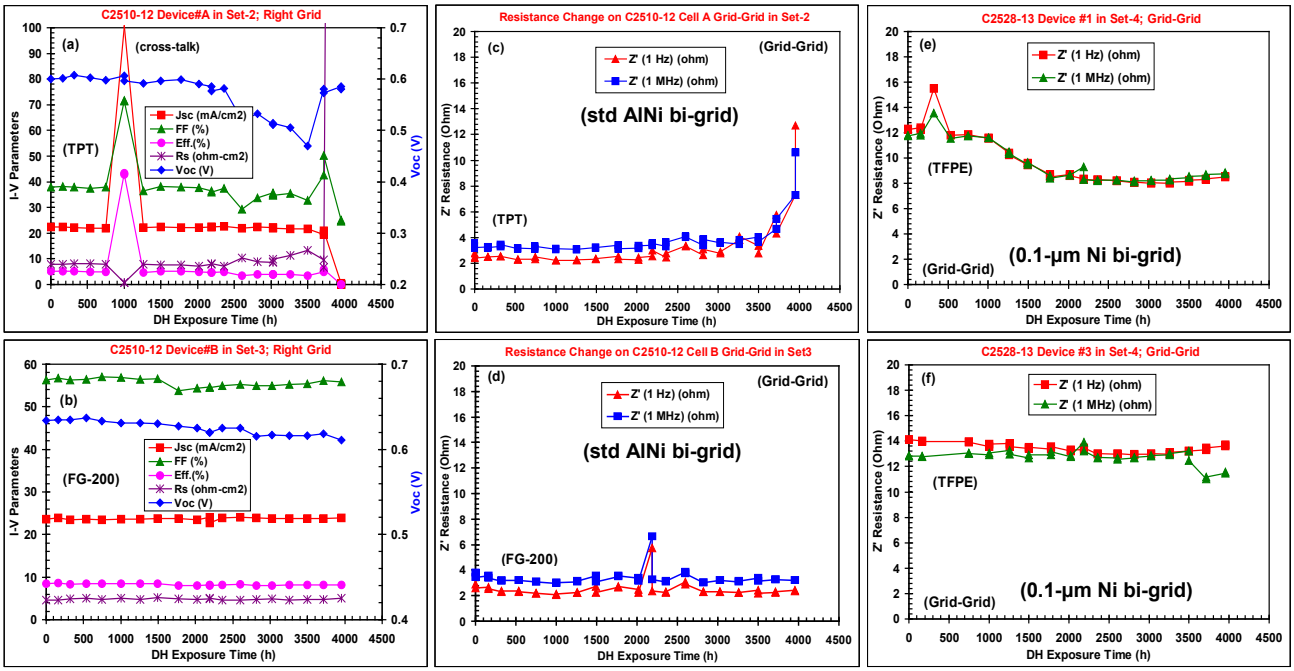

Figure 10. (a, b) I-V parameter plots for C2510-12A in Set-2 with a TPT backsheet and 12B cells in Set-3 with a FG-200 moisture barrier film, respectively, as a function of total DH exposure time. (c, d) Z' resistance plots for BZO on C2510-12A and 12B cells measured via the standard 3.05-µm AlNi bi-grid contacts. (e, f) Z' resistance plots for BZO on cells #1 and #3 of C2528-12 with a TFPE backsheet measured via the 0.1-µm Ni bi-grid contacts.

(figures not shown). In summary, no significant degradation was observed on any of the AZO, BZO/glass, and BZO/CIGS cell sample in Set-4 with a FG-200 moisture barrier film.

4. CONCLUSIONS

A step-stress accelerated degradation testing (SSADT) method was employed for the first time to evaluate the performance reliability of CIGS solar cells and device component materials in four encapsulated Al-framed test structures, using edge sealant and backsheet/moisture barrier film for moisture ingress control. The SSADT exposure used a 15°C and then a 15%RH increment step, beginning from 40°C/40%RH (40/40) to 85°C/70%RH (85/70) for a total DH exposure of 4204 h as of the moment. The voluminous data processed as of DH = 3956 h produced the results as summarized below:

- The CIGS solar cells in Set-1 and 2 encapsulated with a moisture-permeable TPT backsheet exhibited some irregularity in I-V performance degradation pattern. A few cells started to degrade at low T/RH < 55/55, and cross-talk was observed on a few cells producing abnormal high Jsc, either due to incomplete device isolation and/or certain "conductive link" induced by moisture at T/RH < 55/40. Some cells showed large Voc, FF, and efficiency degradation due to increased series Rs (ohm-cm^2) at T/RH ≥ 70/70. Best cells showed nearly identical I-V degradation trend regardless of the AZO thickness on the cells ranging from standard 0.12 μm to 0.50 μm. No clear "stepwise" feature in the I-V parameter degradation curves corresponding to the SSADT T/RH/time profile was observed.

- Results of ECIS analysis indicate degradation of the CIGS solar cells corresponded to increased series resistance Rs (ohm) and degraded p-n junction-related properties, i.e., decrease in parallel (minority carrier diffusion/recombination) resistance Rp, capacitance C, overall time constant ("lifetime") Rp*C, and capacitor quality factor (CPE-P). Heating at 85/70 appeared to benefit the solar cells as indicated by the largely recovered CPE-P factor, but the benefit was offset negatively by Rs increase and Rp decrease.

- Mo and BZO on glass substrates and BZO on CIGS solar cells in Set-1 and -2 (TPT) showed significant degradation with increased resistance at T/RH ≥ 70/70, as measured by ECIS. Exposed at T/RH = 85/70, (i) DH-induced corrosion caused Mo to became brownish with white dot growth and highly resistive; (ii) BZO layers on the CIGS cell pieces with "standard AlNi" bi-grid contact degraded more than on the glass substrates, and showed substantial blistering that was not seen on BZO/glass samples; and (iii) One CdS/CIGS/Mo/SLG sample displyed a small darkening and then flaking feature. Additionally, BZO with standard 3.05-um AlNi contact grid appeared to be less stable than with thin (0.1–0.2 μm) Ni contact grid.

- In Set-3 and 4 with moisture-blocking films (TFPE and FG-200), most CIGS solar cells and device components, i.e., Mo, AZO, BZO, AlNi grid and CdS/CIGS, appeared to be stable at T/RH = 85/70.

- The edge sealant (TruSeal LP101) and moisture-blocking films (TFPE and FG-200) were effective to block moisture ingress as evidenced further by preservation of the initial blue color on the RH indicator strips up to T/RH = 85/70.

The SSADT study is currently ongoing and is to be finished at a final 85/85 DH exposure. A more comprehensive summary will be reported in the near future after the experiment is completed and the voluminous data are thoroughly processed and analyzed; the results may also allow a determination of whether T- and RH-dependent activation energy can be derived for use on the Peck equation.

ACKNOWLEDGEMENTS

The authors thank K. Terwilliger for the WVTR measurements and C. DeHart for assistance in some sample preparations. This work was performed at the National Center for Photovoltaics under DOE Contract No. DE-AC36-08GO28308 with the National Renewable Energy Laboratory.

REFERENCES

[1] I. Repins, M.A. Contreras, B. Egaas, C. DeHart, J. Scharf, C.L. Perkins, B. To, and R. Noufi, "19.9%-Efficient ZnO/CdS/CuInGaSe$_2$ Solar Cell with 81.2% Fill Factor," *Prog. Photovolt: Res. Appl.*, 16, 2008, p. 235.

[2] I. Repins, M. Contreras, M. Romero, Y. Yan, W. Metzger, J. Li, S. Johnston, B. Egaas, C. DeHart, J. Scharf, B. E. McCandless, and R. Noufi, "Characterization of 19.9%-Efficient CIGS Absorbers," *Proc. 33rd IEEE PVSC*, San Diego, CA, May 11-16, 2008.

[3] P. Jackson, D. Hariskos, E. Lotter, S. Paetel, R. Wuerz, R. Menner, W. Wischmann and M. Powalla, "New world record efficiency for Cu(In,Ga)Se$_2$ thin-film solar cells beyond 20%," *Prog. Photovolt: Res. Appl.* 2011; 19:894–897. Published online Jan. 5, 2011 in Wiley Online Library (wileyonlinelibrary.com). DOI: 10.1002/pip.1078; pp. 894-897

[4] K. Whitfield, "Common Failure Modes for Thin-Film Modules and Considerations toward Hardening CIGS Cells to Moisture – A "Suggested" Topic," *Proc. 2010 PV Module Reliability Workshop*, Feb. 16-17, 2010, Golden, CO.

[5] A. Preiss, S. Krauter, M. Schoppa, and I. Luck, "PV Module Testing – How to Ensure Quality after PV Module Certification," *Photovoltaic International*, 13th ed., August, 2011, pp. 166-176.

[6] J. Pern and R. Noufi, "An Investigation of Stability Issues of ZnO and Mo on Glass Substrates for CIGS Solar Cells upon Accelerated Weathering and Damp Heat Exposures," DOE SETP Review Meeting, Denver, CO., April 17-19, 2007. http://www1.eere.energy.gov/solar/review_meeting/pdfs/ p_9_pern_nrel.pdf.

[7] F.J. Pern, R. Noufi, X. Li, C. DeHart, and B. To, "Damp-Heat Induced Degradation of Transparent Conducting Oxides for Thin-Film Solar Cells", *Proc. 33rd IEEE PVSC*, San Diego, CA, May 11-16, 2008.

[8] R. Sundaramoorthy, F.J. Pern, C. DeHart, T. Gennett, F.Y. Meng, M. Contreras, and T. Gessert, "Stability of TCO Window Layers for Thin-Film CIGS Solar Cells upon Damp Heat Exposures – Part II," *Proc. 2009 SPIE Conference: Reliability of PV Cells, Modules, Components, and Systems*, Aug. 2-6, 2009, San Diego, CA.

[9] F.J. Pern, S.H. Glick, X. Li, C. DeHart, T. Gennett, M. Contreras, and T. Gessert, "Stability of TCO Window Layers for Thin-Film CIGS Solar Cells upon Damp Heat Exposures – Part III," *Proc. 2009 SPIE Conference: Reliability of PV Cells, Modules, Components, and Systems*, Aug. 2-6, 2009, San Diego, CA.

[10] F.J. Pern, B. Egaas, B. To, C.-S. Jiang, J.V. Li, S. Glynn, and C. DeHart, "A Study on the Humidity Susceptibility of Thin-Film CIGS Absorber," *Proc. 34 IEEE PVSC*, June 7-12, 2009, Philadelphia, PA.

[11] F.J. Pern, S.H. Glick, R. Sundaramoorthy, B. To, X. Li, C. DeHart, S. Glynn, T. Gennett, R. Noufi, and T. Gessert, "Damp-Heat Instability and Mitigation of ZnO-Based Thin Films for CuInGaSe$_2$ Solar Cells," *Proc. 35 IEEE PVSC*, June 20-25, 2010, Honolulu, Hawaii.

[12] R. Feist, S. Rozeveld, M. Mushrush, R. Kaley, B. Lemon, J. Gerbi, B. Nichols, R. Nilsson, T. Richardson, S. Sprague, R. Tesch, S. Torka, C. Wood, S. Wu, S. Yeung, and M. T. Bernius, "Examination of Lifetime-Limiting Failure Mechanisms in CIGSS-based PV Minimodules under Environmental Stress," *Proc. 33th IEEE PVSC*, May 11-16, 2008, San Diego, CA.

[13] R. Feist, S. Rozeveld, B. Kern, J. D'Archangel, S. Yeung, and M. Bernius, "Further Investigation of The Lifetime-Limiting Failure Mechanisms of CIGSS-Based Minimodules Under Environmental Stress," *Proc. 34th IEEE PVSC*, June 7-12, 2009, Philadelphia, PA.

[14] R. Sundaramoorthy, I. Repins, D. Albin, J. Pern, X. Li, T. Gessert, T. Gennett, "Investigation of Stability Issues of TCO Barrier Layers for CIGS Devices during Damp Heat and Dry Heat Exposures," *Bulletin of APS*, Vol. 54, paper # X12.00002, March 16-20, 2009, Pittsburgh, PA.

[15] E. Suhir, "Accelerated Life Testing and Probabilistic Design for Reliability, Part I: Accelerated Life Testing and Part II: Probabilistic Design for Reliability." Tutorial at the 2010 ASTR Workshop, October 6-8, 2010 Denver, CO.

[16] E. Suhir, "Accelerated Life Testing (ALT) in Microelectronics and Photonics: Its Role, Attributes, Challenges, Pitfalls, and Interaction with Qualification Tests," ASME, *J. Electronic Packaging*, 124, 2002, pp. 281-291.

[17] I. H. Khamis, "Comparison between Constant and Step-Stress Tests for Weibull Models," *International Journal of Quality & Reliability Management*, 14, 1997, pp. 74-81.

[18] S.-T. Tseng and Z.-C. Wen, "Step-Stress Accelerated Degradation Analysis for Highly Reliable Products, *J. Quality Technology*, 32, 2000, pp. 209-216.

[19] W. Jones and R. Elmore, "A New Reliability Testing Technique for Photovoltaic Deices and Cells: Step-Stress Accelerated Degradation Testing," NREL FY2011 LDRD pre-proposal.

[20] J. Lee, P. Hacke, D. Jordan, W. Jones," Determining Lifetime of Solar Modules for Temperature-Humidity Driven Failures: A Step Stress Accelerated Lifetime Method." December 17, 2009, NREL pre-proposal.

[21] J. Lee, R. Elmore, C. Suh and W. Jones, "Step-Stress Accelerated Degradation Testing (SSADT) for Photovoltaic (PV) Devices and Cells," *Proc. 2010 IEEE ASTR (Accelerated Stress Testing & Reliability)*, October 6-8, 2010, Denver, CO. (Components, Packaging, and Manufacturing Technology Society, CPMT)

[22] J. Lee, R. Elmore, and W. Jones, "Statistical Modeling of Photovoltaic Reliability using Accelerated Degradation Techniques," *Proc. 2011 PV Module Reliability Workshop*, NREL, Golden, CO

[23] F.J. Pern, L. Mansfield, C. DeHart, S.H. Glick, F. Yan, and R. Noufi, "Thickness Effect of Al-Doped ZnO Window Layer on Damp-Heat Stability of $CuInGaSe_2$ Solar Cells," *Proc. 37th IEEE PVSC*, June 21-25, 2011, Seattle, WA.

[24] F.J. John Pern and R. Noufi, "Characterization of Damp-Heat Degradation of $CuInGaSe_2$ Solar Cell Components and Devices by (Electrochemical) Impedance Spectroscopy," *Proc. 2011 SPIE Conference: Reliability of PV Cells, Modules, Components, and Systems*, August 22-25, 2011, San Diego, CA.

[25] Materion's "Moisture Barrier Films" technical brochure LAC Barrier Films, Rev. 020311 (in which the unit uses gm/cm^2/day incorrectly). The WVTR data with correct unit is seen on "FG-200 Solar Module Vapor Barrier Films," http://materion.com/Products/ProductGroups/ThinFilmCoatings/VaporBarrierFilms/FG-200SolarModuleVaporBarrierFilms.aspx.

[26] Jinsuk Lee, personal communications and discussions while Lee was still at NREL.

[27] F.J. Pern, F. Yan, K. Zaunbrecher, B. To, J. Perkins, and R. Noufi, "Investigation of Some Transparent Metal Oxides as Damp Heat Protective Coating for CIGS Solar Cells," Proc. 2012 *SPIE Conference: Reliability of PV Cells, Modules, Components, and Systems*, August 12-16, 2012, San Diego, CA.

[28] I. Mora-Sero, G. Garcia-Belmonte, P.P. Boix, M.A. Vazquez, and J. Bisquert, "Impedance spectroscopy Characterisation of Highly Efficient Silicon Solar Cells under Different Light Illumination Intensities," *Energy Environ. Sci.*, 2, 2009, pp. 678–686.

[29] J. Bisquert, "Impedance Spectroscopy Applied on Solar Cells," a presentation at the *Nordic Workshop on Solar Electricity*, April 27-29 2004, Sonnerupgaard Gods, Denmark.

[30] J. Bisquert, "Theory of the Impedance of Electron Diffusion and Recombination in a Thin Layer," *J. Phys. Chem. B*, 106, 2002, pp. 325-333.

[31] *Impedance Spectroscopy – Emphasizing Solid Sate Materials and Systems*, J. Ross MacDonald ed., John Wiley & Sons, New York, 1987. Also see "Constant Phase Element" in Chapters 1 and 2.

[32] H. Bayhan and A. S. Kavasoglu, "Admittance and Impedance Spectroscopy on $Cu(In,Ga)Se_2$ Solar Cells, *Turk J. Phys.,* 27, 2003, pp. 529-535.

[33] H. Bayhan and A. S. Kavasoglu, "Study of $CdS/Cu(In,Ga)Se_2$ Heterojunction interface Using Admittance and Impedance Spectroscopy," *Solar Energy*, 80, 2006, pp. 1160-1164.

[34] A. Meier, S.H. Glick, and F.J. Pern, "Impedance Spectroscopy as a Non-Invasive Analytical Method for Monitoring Solar Cell Degradation," NCPV Photovoltaics Program Review, *Proc. of 15th Conference*, M. Al-Jassim, J.P. Thornton, and J. M. Gee ed., CP462, Denver, CO, Sept., 1999, pp. 661-666. American Institute of Physics, Woodbury, New York.

[35] (a) "Constant phase element," http://en.wikipedia.org/wiki/Constant_phase_element. (b) "Explaining a Constant Phase Element (CPE)," http://www.consultrsr.com/resources/eis/cpe2.htm, and the references therein. (c) Help menu on equivalent circuits, instant curve-fitting function and constant phase element in the ZView program (ver. 3.2c) from Scribner Associates, Inc.